

“Rosenbluth” separation of the  $J/\psi$  near-threshold photoproduction - an access to the  
gluon Gravitational Form Factors at high  $t$

Lubomir Pentchev\* and Eugene Chudakov†

### Abstract

We perform analysis of the near-threshold  $J/\psi$  photoproduction data off the proton based on the high skewness expansion ( $\xi \rightarrow 1$ ) of the cross-section in Ref. [1]. This expansion allows to separate the corresponding gluonic form factors, in much the same way as this is done in the electromagnetic case with the Rosenbluth separation. We examine the independence of the extracted form factors with the photon beam energy. In Ref. [1] these form factors, in the leading-moment approximation, are related to the proton’s gluon Gravitational Form Factors (gGFF). Using this approximation, we compare the extracted data points with lattice calculations in the region of momentum transfer squared of  $1 < |t| < 2 \text{ GeV}^2$ , where the data and lattice results overlap. Such analysis demonstrates the possibility of extracting some combinations of the gGFFs from the data at high  $t$ , complementary to the lattice calculations available in the low  $t$  region. However, higher statistics is needed to more accurately check the predicted  $\xi$ -scaling behavior of the data and compare with the lattice results, thus testing the theoretical assumptions used in Ref. [1].

---

\* Thomas Jefferson National Accelerator Facility, Newport News, Virginia 23606, USA; pentchev@jlab.org

† Thomas Jefferson National Accelerator Facility, Newport News, Virginia 23606, USA; gen@jlab.org

## I. INTRODUCTION

The charmonium photoproduction near threshold provides a unique way to probe the gluonic structure of the nucleon. Due to the high mass of the charm quark and proximity to the threshold, the reaction is expected to be dominated by two-gluon exchange [2, 3]. In addition, assuming factorization where the hard scale is defined by the high charmonium mass, the process involves the gluonic Generalized Parton Distribution (GPD) of the nucleon [4, 5]. As the two gluons can mimic graviton-like exchange, the gluonic GPD in turn can be related to the gluon Gravitational Form Factors (gGFFs) [4, 6]. To be able to access the gluonic content of the nucleon, the above chain of assumptions requires experimental testing.

In the recent years, thanks to the 12 GeV Jefferson Lab electron accelerator, several experiments measured the  $J/\psi$  photoproduction near threshold with much higher precision than the previous experiments from the 1970s. The GlueX experiment in Hall D performed measurements with nearly full acceptance spectrometer in a wide range of the photon beam energy starting from the threshold of 8.2 GeV to the maximum available energy of about 11.8 GeV [7, 8]. In addition to the total cross-section, the differential cross sections were extracted in three slices of the photon beam energy, providing full coverage of the near-threshold kinematic region. The  $J/\psi$ -007 experiment in Hall C accumulated similar statistics in a narrower kinematic region with several settings of their two low-acceptance spectrometers that however allowed very high luminosity [9]. The differential cross sections were measured in 10 narrow energy bins with very high statistics in the forward region.

In Ref. [9] the gGFFs have been extracted by fitting the  $J/\psi$ -007 data with the theoretical predictions from the holographic [10] and GPD [4] approaches. Note that the fits used the full  $J/\psi$ -007 data set dominated by the cross sections at low  $|t|$ . In the GPD analysis of Ref. [5], the data from both GlueX and  $J/\psi$ -007 experiments were used to extract the gGFFs. The GPD approach is based on expansion in the skewness parameter<sup>1</sup> for  $\xi \rightarrow 1$  (see also [6]) therefore its validity is justified for high  $|t|$  values (due to kinematic correlation between  $t$  and  $\xi$ ). A common feature of the above two analyses in Refs. [5, 9] is the modeling of the gGFFs with dipole/tripole functions, as proposed in Ref. [11] in analogy with the electro-magnetic

---

<sup>1</sup> The skewness is one of the three GPD variables (in addition to  $t$  and the parton longitudinal momentum fraction  $x$ ) defined as the longitudinal momentum transfer fraction - see Eq.(7) in Ref. [4]

form factors. The choice of this functional form comes also from the parametrization of the lattice results in Refs. [12, 13] so that some parameters in these parametrizations can be fixed from the lattice calculations when fitting the data. While the GPD approach works at high  $|t|$ , the lattice calculations of the gGFFs have been done so far in the  $0 < |t| < 2 \text{ GeV}^2$  region. Therefore, using the lattice parametrization of the gGFFs and assuming the same functional form to extend to high  $|t|$  may result in significant bias.

The analysis in this work is based on one of the important results of Ref. [1], that the matrix element squared of the charmonium photoproduction for high  $\xi$  values can be presented in this general form:

$$|G(\xi, t)|^2 = \xi^{-4} [G_0(t) + \xi^2 G_2(t) + \xi^4 G_4(t)], \quad (1)$$

where  $G_0$ ,  $G_2$ , and  $G_4$  are functions only of  $t$ , they are related to the gluonic Compton-like Form Factors (gCFFs). We aim to extract the individual terms in Eq.(1) from the experimental data with some minimal additional assumptions. In contrast to the studies in Refs. [5, 9], **the results of the procedure in this work will not be model functions fitted to the data, but actual data points measuring the  $t$ -dependence of the above form factors.**

We point out the analogy with the Rosenbluth separation of the electric,  $G_E$ , and magnetic,  $G_M$ , form factors. Based on the Rosenbluth formula [14] for the electron-proton elastic cross section,  $d\sigma/d\Omega$ , the method relies on the linear dependence of the reduced cross section,  $\sigma_R$ , on the kinematic variable  $\epsilon$ :

$$\sigma_R = \frac{d\sigma}{d\Omega} / \left( \frac{d\sigma}{d\Omega} \right)_M \frac{\epsilon(1+\tau)}{\tau} = \frac{\epsilon}{\tau} G_E^2(t) + G_M^2(t), \quad (2)$$

where  $\left( \frac{d\sigma}{d\Omega} \right)_M$  is the Mott cross section,  $\tau = -t/4m^2$ , where  $m$  is the proton mass. By measuring  $\sigma_R$  at the same momentum transfer  $t$  as function of  $\epsilon/\tau$ , one can estimate the slope and the intercept, being respectively the electric and magnetic form factors squared at this value of  $t$ .

The analogy of Eq.(1) with Eq.(2) is clear: instead of  $\epsilon$ , we can use the variations with  $\xi$  at

a fixed  $t$  to extract the form factors in Eq.(1). In this paper we will apply a similar “Rosenbluth” technique, however with some noticeable differences. Due to the limited experimental data so far, it is practically impossible to analyze separately data sets in narrow ranges of  $t$  versus some function of  $\xi$ . At the same time global analysis of the data is complicated due to kinematic constraints that impose correlations between the ranges of  $t$  and  $\xi$ .

In our analysis we will use the results from the two Jefferson Lab experiments, GlueX and  $J/\psi$ -007, selecting data points with  $\xi > 0.4$ . Such limit may not be high enough for the assumptions in Ref. [1] to be valid, and the selection is driven by the limited amount of data at high  $\xi$ . In addition we will select measurements with photon energies above 9.3 GeV, to stay away from the open-charm thresholds of  $\Lambda_c \bar{D}$  and  $\Lambda_c \bar{D}^*$ . As discussed recently in Refs.[8, 15, 16], there is possible evidence for contributions from reactions with open-charm exchange.

In section II we will formulate the “Rosenbluth” technique. It will be used in section III to extract the  $G_0(t)$  and  $G_2(t)$  form factors and check the energy independence of the results. In section IV we will work within the leading-moment approximation to demonstrate the possibility of extracting some combinations of the gGFFs and compare them to the lattice results. Some additional remarks and summary will be given in section V.

## II. THE “ROSENBLUTH” TECHNIQUE

In Ref. [1] the differential cross section of the  $J/\psi$  photoproduction near threshold is presented as a function of the skewness parameter  $\xi$  and the momentum transfer  $t$ :

$$\frac{d\sigma}{dt}(\xi, t) = \frac{\alpha e_q^2}{4(W^2 - m^2)^2} \frac{(16\pi\alpha_S)^2}{3M^3} |\Psi_{NR}(0)|^2 \cdot |G(\xi, t)|^2 = F \cdot |G(\xi, t)|^2, \quad (3)$$

where the factor  $F$  includes a kinematic factor and the  $J/\psi$  non-relativistic wave function at origin,  $\Psi_{NR}(0)$ , and depends only on the photon beam energy,  $E$ . The matrix element squared,  $|G(\xi, t)|^2$ , given in Eq.(1), has three terms related to the gluonic Compton Form

Factors (gCFF),  $\mathcal{A}_g$ ,  $\mathcal{B}_g$ , and  $\mathcal{C}_g$ , as:

$$G_0(t) = (\mathcal{A}_g(t))^2 - \frac{t}{4m^2} (\mathcal{B}_g(t))^2 \quad (4)$$

$$G_2(t) = 2\mathcal{A}_g(t)\mathcal{C}_g(t) + 2\frac{t}{4m^2}\mathcal{B}_g(t)\mathcal{C}_g(t) - (\mathcal{A}_g(t) + \mathcal{B}_g(t))^2 \quad (5)$$

$$G_4(t) = \left(1 - \frac{t}{4m^2}\right) (\mathcal{C}_g(t))^2. \quad (6)$$

From Eqs.(3) and (1) we construct the reduced cross section:

$$\sigma_{R0}(E, t) = \frac{d\sigma}{dt}(E, t) \frac{\xi^2(E, t)}{F(E)} = \xi^{-2}(E, t)G_0(t) + G_2(t) + \xi^2(E, t)G_4(t), \quad (7)$$

where we have indicated the energy and  $t$  dependence of the corresponding variables<sup>2</sup>. We have verified, initially based on the lattice results from Refs. [12, 13] discussed later, that the last term in Eq.(1), and respectively Eq.(7), is much smaller in absolute value than each of the other two terms. Partially this is because of the  $\xi^4/\xi^2$  suppression factor (as  $\xi < 1$ ) with respect to the first/second term. This assumption will be checked later based on the results of this analysis. Note that this does not necessarily mean that the last term in Eqs.(1) and (7) can be neglected. It will be shown that the other two terms have different signs and it is possible they largely cancel each other.

The second term in Eq.(7) depends only on  $t$  and we can eliminate it by taking the difference of the cross sections at two different photon energies,  $E_i$  and  $E_j$ :

$$\begin{aligned} \sigma_{R0}(E_i, t) - \sigma_{R0}(E_j, t) &= [\xi^{-2}(E_i, t) - \xi^{-2}(E_j, t)] G_0(t) \\ &+ [\xi^2(E_i, t) - \xi^2(E_j, t)] G_4(t). \end{aligned} \quad (8)$$

Now the last term can be neglected with respect to the first one, and we have the  $G_0$  function extracted from experimental data:

$$G_0^{exp.}(t) = [\sigma_{R0}(E_i, t) - \sigma_{R0}(E_j, t)] / [\xi^{-2}(E_i, t) - \xi^{-2}(E_j, t)] \quad (9)$$

---

<sup>2</sup> Note that all reduced cross sections defined in this work are dimensionless quantities

We will choose a data set at a given energy  $E_i$  as a reference. Thus, the above equation will give us the slope of the reduced cross section as function of  $\xi^{-2}$  for each additional data point with transfer momentum  $t$  and energy  $E_j$  with respect to the reference energy, for which the slope is  $G_0(t)$ . With this method the uncertainties of the reference data set can be considered to be systematic errors common for all data points.

In much the same way we can extract  $G_2(t)$  in Eq.(1) as:

$$G_2^{exp.}(t) = [\sigma_{R2}(E_i, t) - \sigma_{R2}(E_j, t)] / [\xi^2(E_i, t) - \xi^2(E_j, t)], \quad (10)$$

where we have defined another reduced cross section as:

$$\sigma_{R2}(E, t) = \frac{d\sigma}{dt}(E, t) \frac{\xi^4(E, t)}{F(E)} \quad (11)$$

### III. ENERGY INDEPENDENCE OF THE FORM FACTORS

The practical implementation of the above technique is limited by the quality and range of the available data. The data sets from the two Jefferson Lab experiments are illustrated in Fig.1. As discussed above for the main part of our analysis we will use the data with  $\xi > 0.4$  and  $E > 9.3$  GeV. This region on the  $E$ -vs- $t$  plane in Fig.1 is shown with color. We will choose the highest energy data set from the GlueX experiment, at an average energy  $E_i = 10.82$  GeV, as a reference and subtract the other data at different energies  $E_j$ . Such a choice gives maximum leverage in  $\xi$  when calculating the slopes from Eqs.(9) and (10), at the same time the highest energy data set is more precise and has the widest range in  $t$ .

In principle, we can fit the reference reduced cross section with some function without any model, so that we can use it in Eqs.(9) and (10) to subtract the reduced cross sections at the  $t$  values of the data points at the other energies. Still, as seen in Fig.1, due to the  $\xi > 0.4$  constraint, the  $1 - 2$  GeV<sup>2</sup> region in  $|t|$  is not covered by the reference cross section, therefore it requires extrapolation to lower  $|t|$ . For that we will use the results from Ref. [1] in the leading-moment approximation to fit all the data simultaneously. An alternative model-independent approach will be discussed later. In the leading-moment approximation

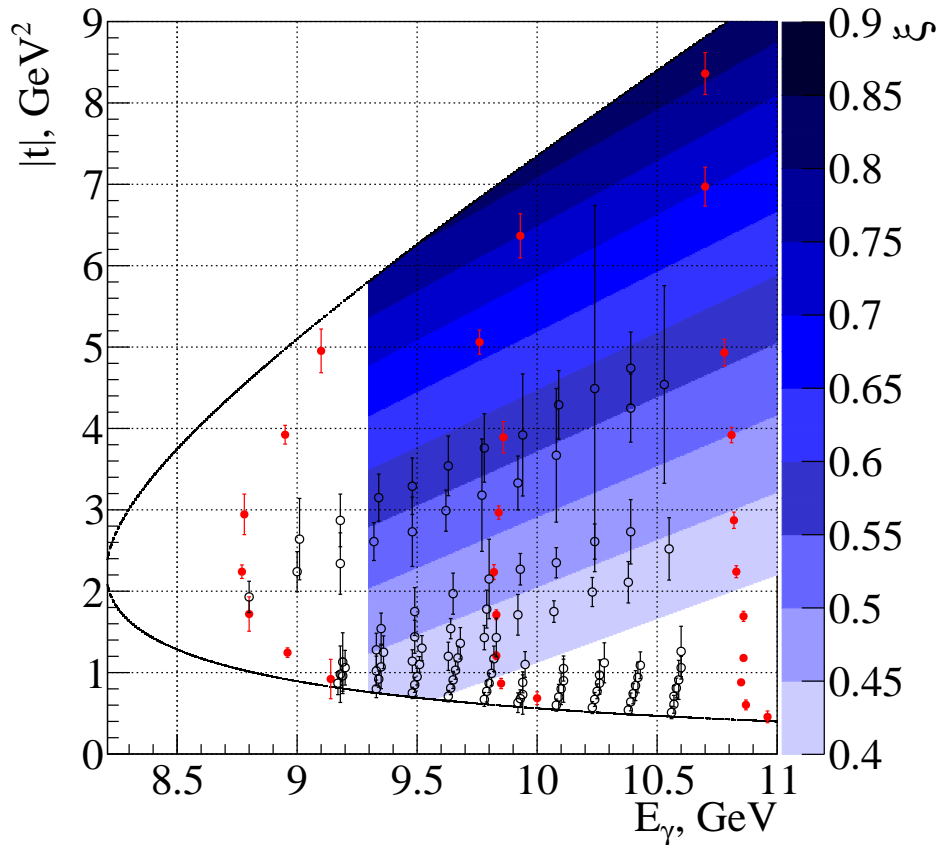


FIG. 1: Data points of the GlueX [8] (red solid) and  $J/\psi$ -007 [9] (black open) experiments on the  $E$ -vs- $t$  plane. The vertical error bars represent the relative errors of the differential cross sections measured at these points in arbitrary units (not related to the  $y$  axis). The  $\xi$  values on this plot are given on the  $z$ -axis (color coded). Some of the  $J/\psi$ -007 points are slightly shifted up in energy for visibility. The colored (shaded in print) area corresponds to the  $\xi > 0.4$  and  $E > 9.3$  GeV region that is used in this analysis.

the gCFFs  $\mathcal{A}_g$ ,  $\mathcal{B}_g$ , and  $\mathcal{C}_g$  in Eqs.(4-6) are related to the gluonic Gravitational Form Factors (gGFF)  $A_g$ ,  $B_g$ , and  $C_g$  as:

$$\mathcal{A}_g(t) = 2A_1^{conf} A_g(t) \quad (12)$$

$$\mathcal{B}_g(t) = 2A_1^{conf} B_g(t) \quad (13)$$

$$\mathcal{C}_g(t) = 8A_1^{conf} C_g(t), \quad (14)$$

using the conformal expansion of the gCFFs where  $A_1^{conf} = 5/4$  [1]. For this fit we use a tripole parametrization for all three gGFFs,  $F_g(0)/(1 - t/m_g^2)^3$ , each with two parameters,

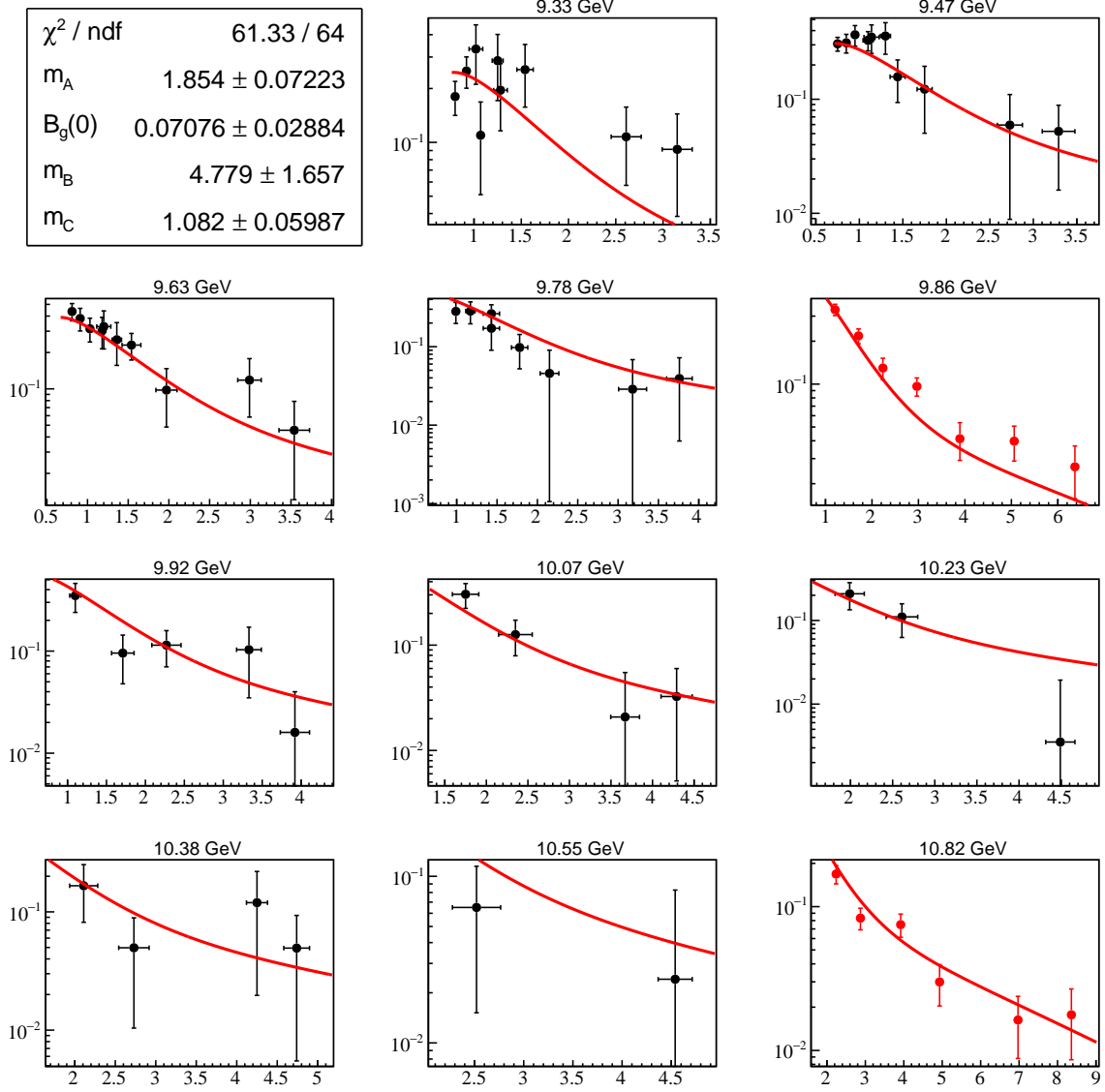


FIG. 2: Global four-parameter fit of the reduced cross sections,  $\xi^2/F \cdot d\sigma/dt$ , as function of  $|t|$  (in  $\text{GeV}^2$ ), using the model of Ref.[1], from GlueX (red) and  $J/\psi$ -007 (black) experiments for different photon energies as indicated. For the further analysis only the fitted function at 10.82 GeV is used.

the form factor at  $t = 0$ ,  $F_g(0)$ , and the mass scale,  $m_g$ . We also fix:

$$A_g(0) = 0.414 \quad (15)$$

$$C_g(0) = -0.642 \quad (16)$$

from the CT18 global analysis of the parton distribution functions [17] for  $A_g(0)$ , and lattice

results in Ref. [13] for  $C_g(0)$ , keeping the two parameters for  $B_g$  free. In Refs.[5, 9] when extracting the gGFFs,  $B_g$  is neglected based on the lattice results for  $|t| < 2 \text{ GeV}^2$ . Here we will keep it as it improves the fit quality at high  $|t|$ . We demonstrate this procedure when fitting the reduced cross section,  $\sigma_{R0}$ , as function of  $t$  for all energies using Eq. (7), where the  $G$  functions are taken from Eqs.(4-6,12-14). The results of this global fit are shown in Fig.2 exhibiting a good fit quality. In the further analysis for the extraction of  $G_0^{exp.}(t)$ , in Eq.(9) we will use only the fitted function for the reference energy  $E_i = 10.82 \text{ GeV}$  (Fig.2 bottom right). The global fit of the other reduced cross section,  $\sigma_{R2}$ , gives very similar results, from which fit only the fitted function for the reference energy will be used in Eq.(10) to extract  $G_2^{exp.}(t)$ .

To illustrate clearly how the ‘‘Rosenbluth’’ technique works, in Fig. 3 we show the different stages of the extraction of the  $G_0(t)$  function from the GlueX data. Here, just for this demonstration, we have included the differential cross section at the lowest beam energy. Starting from the original cross sections, going to the  $\xi$ -scaled cross sections, and finally calculating the slopes from Eq.(9), it is remarkable to see how the results at the different energies converge into a function,  $G_0^{exp.}(t)$ , that is largely energy independent.

The results for  $G_0^{exp.}$  and  $G_2^{exp.}$  using all the data are shown in Figs. 4a and 4b. We see that the extracted functions do not depend on energy within the experimental errors. Numerically, this is confirmed by the good quality of the fit of all the data using a dipole function. The uncertainties of the fitted function at the reference energy (as in Fig. 2 bottom right panel) are scaled by the factors in Eqs.(9,10) and shown in Figs.4a and 4b as global systematic errors.

While we applied the GPD model of Ref. [1] in the leading-moment approximation to fit all the data, in the above procedure we have only used the fitted function for the reference energy mainly to extrapolate the reduced cross section from  $|t| \sim 2 \text{ GeV}^2$ , where the lowest- $|t|$  data point is, down to  $|t| \sim 1 \text{ GeV}^2$  - see the curve in the middle panel in Fig.3. We found that similar results can be obtained when fitting only the reference reduced cross section (though with bigger fit uncertainties) with some model-independent function if its value is fixed at a point  $|t| \leq 1 \text{ GeV}^2$  by some model constraints like Eqs.(15,16), which are important for the extrapolation to the lower  $|t|$  region. Nevertheless, when enough statistics is available,

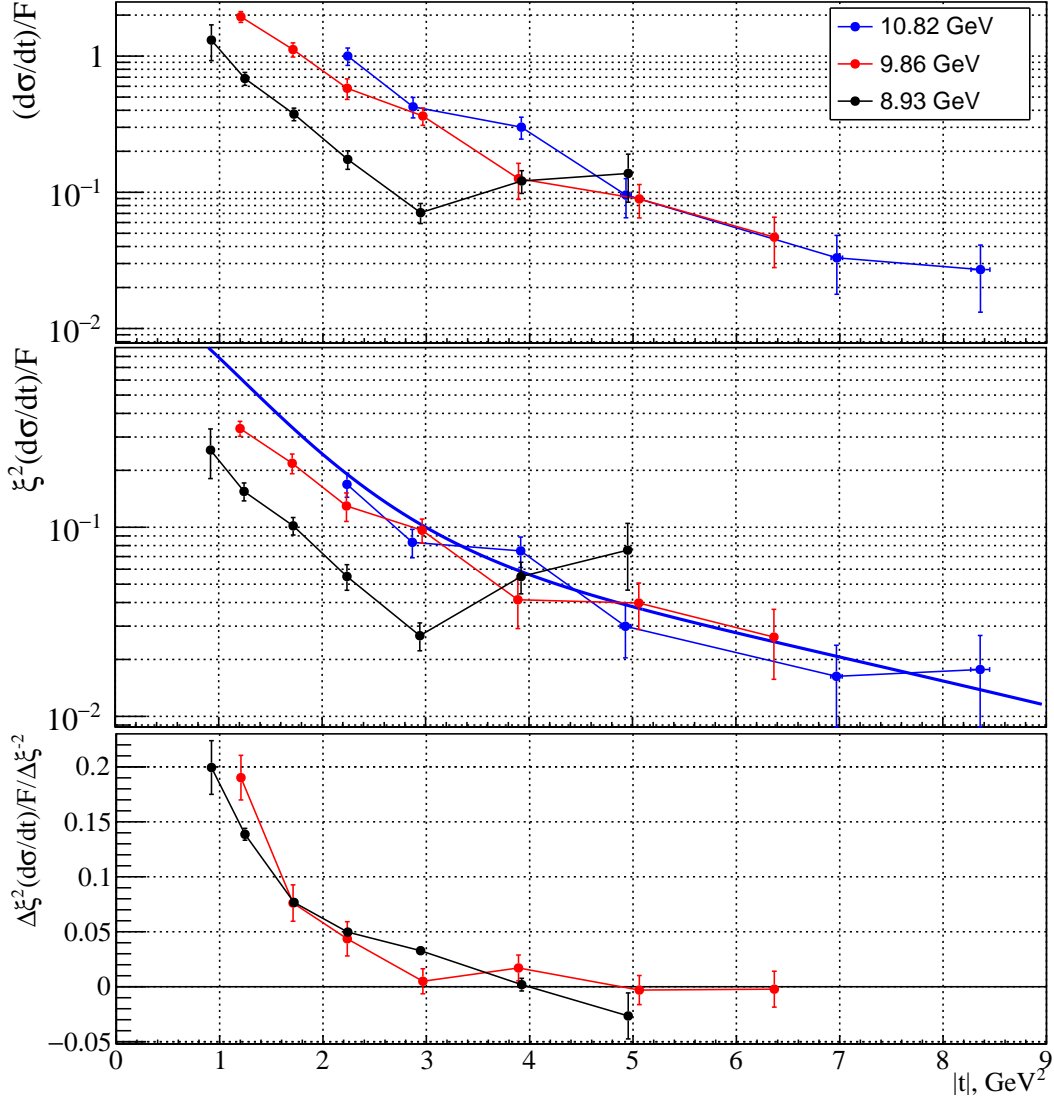
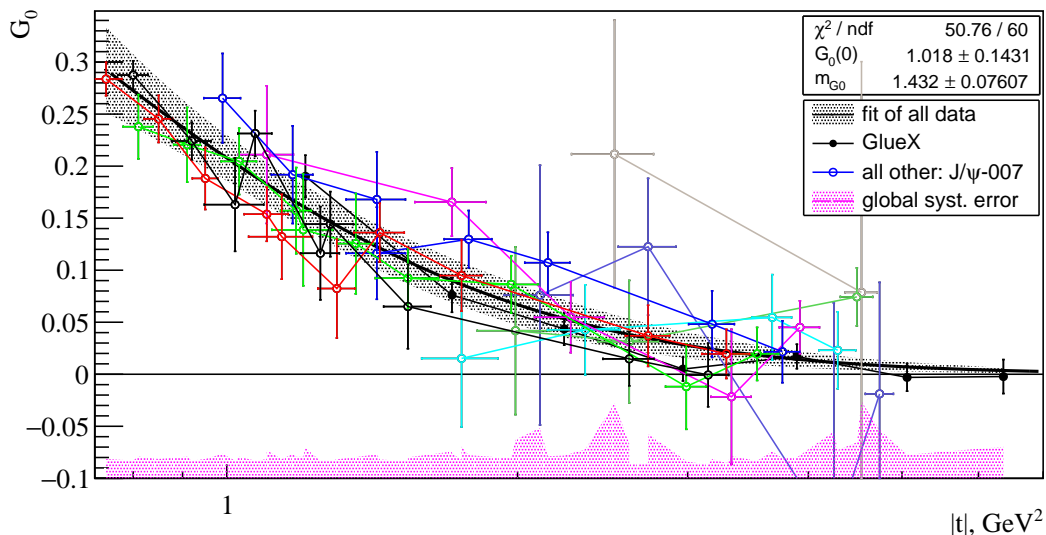
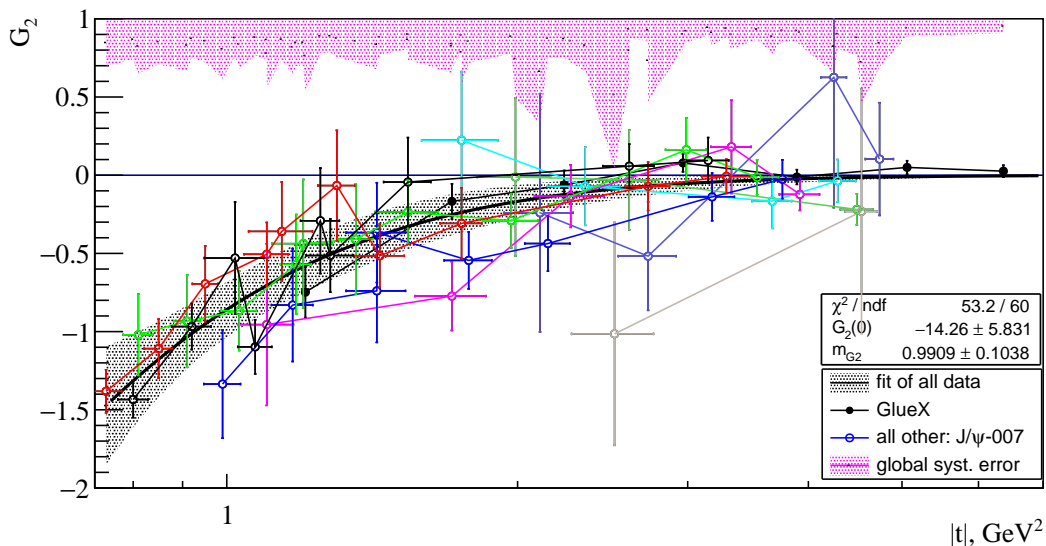


FIG. 3: Different stages of applying the “Rosenbluth” extraction of the  $G_0(t)$  function using the GlueX data: the differential cross sections at three energy slices normalized by  $F(E)$  - see Eq.(3) (top), the reduced cross sections - Eq.(7) (middle), and the extracted  $G_0(t)$  function with Eq.(9) using the highest energy as a reference (bottom). The fitted function of the reduced cross section at the highest energy from the global fit (Fig.2 bottom right), is shown in the middle panel (blue curve), as well. The points are connected with lines to guide the eye only.

it would be possible to chose a free parameter that constrains the fit of the reference cross section at some  $t$  value. We determine this parameter by minimizing the  $\chi^2$  of the fits of  $G_0(t)$  and  $G_2(t)$ , i.e. requiring  $G_0(t)$  and  $G_2(t)$  to be energy independent.



(a)



(b)

FIG. 4:  $G_0(t)$  (top) and  $G_2(t)$  (bottom) functions as extracted from the GlueX (solid) and  $J/\psi$ -007 (open symbols) data for  $\xi > 0.4$  using Eqs.(9,10) for different photon beam energies (different colors connected with lines). The data are fitted with dipole functions squared,  $G(0)/(1 - t/m_G^2)^4$ , shown with one-sigma error band.

#### IV. RELATION TO THE GLUON GRAVITATIONAL FORM FACTORS

In this section we will use the leading-moment approximation of Ref. [1] that relates the  $G$  form factors in Eq.(1) to the gluon Gravitational Form Factors, as given by Eqs.(4-6) and

Eqs.(12-14). In Fig.5a and Fig.5b, we compare our results from the previous section to the calculations of  $G_0$  and  $G_2$  in the leading-moment approximation using the lattice results for the gGFFs from Ref. [13]. We see a good agreement between the lattice and experimental results in the common  $1 - 2 \text{ GeV}^2$  region, especially for  $G_0$ . However, this is partially a result of the constraints from Eqs.(15,16), as discussed above. To demonstrate the deviation from the  $\xi$ -scaling, in addition to the data with  $\xi > 0.4$  used in the analysis, we show also the results for  $\xi < 0.4$ . Notably, the  $\xi < 0.4$  data points for both  $G_0$  and  $G_2$  exhibit larger spread and deviate significantly from the lattice calculations.

The  $A_g$  form factor squared is proportional to  $G_0$  due to the small  $B_g^2$  contribution (see Eqs.(4,12)) and can be extracted from the experimental data for  $|t| > 1 \text{ GeV}^2$ . We can use the above results for  $G_0$  and  $G_2$  to estimate the  $C_g$  form factor from Eqs.(4,5,12,13). However, as the calculations of  $G_0$  and  $G_2$  use the same data, the best way to do this is to extract directly the sum  $G_0 + G_2$  in which  $A_g^2$  cancels out. For that we rearrange Eq.(7) as:

$$\begin{aligned} \frac{d\sigma}{dt}(E, t) \frac{1}{F(E)} \frac{\xi^4(E, t)}{1 - \xi^2(E, t)} &= G_0(t) + \frac{\xi^2(E, t)}{1 - \xi^2(E, t)} (G_0(t) + G_2(t)) \\ &+ \frac{\xi^4(E, t)}{1 - \xi^2(E, t)} G_4(t). \end{aligned} \quad (17)$$

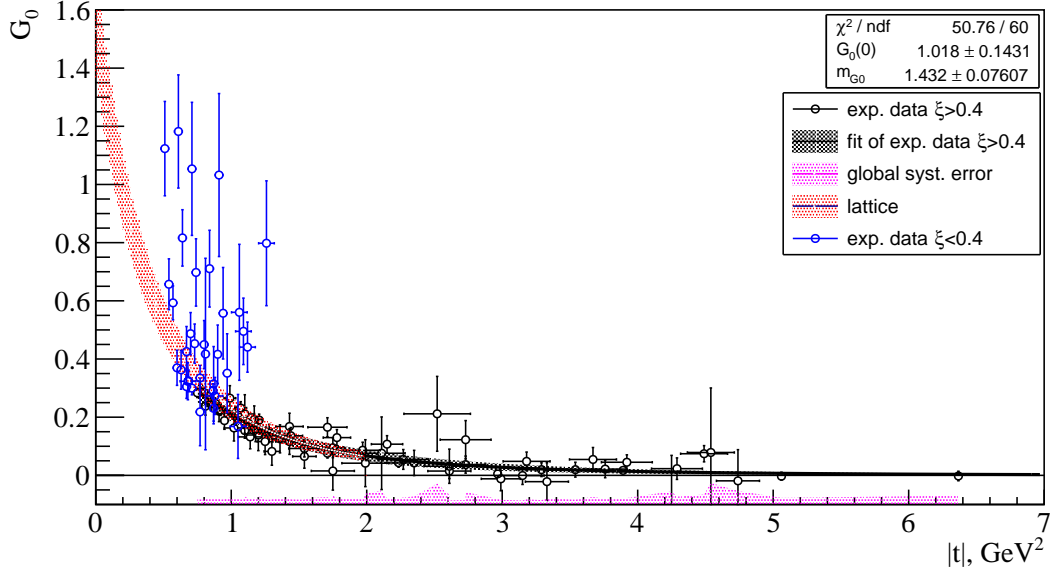
In much the same way as for  $G_0^{exp.}(t)$  and  $G_2^{exp.}(t)$ , we can extract  $G_0 + G_2$  as:

$$(G_0(t) + G_2(t))^{exp.} = [\sigma_{R02}(E_i, t) - \sigma_{R02}(E_j, t)] / \left[ \frac{\xi^2(E_i, t)}{1 - \xi^2(E_i, t)} - \frac{\xi^2(E_j, t)}{1 - \xi^2(E_j, t)} \right], \quad (18)$$

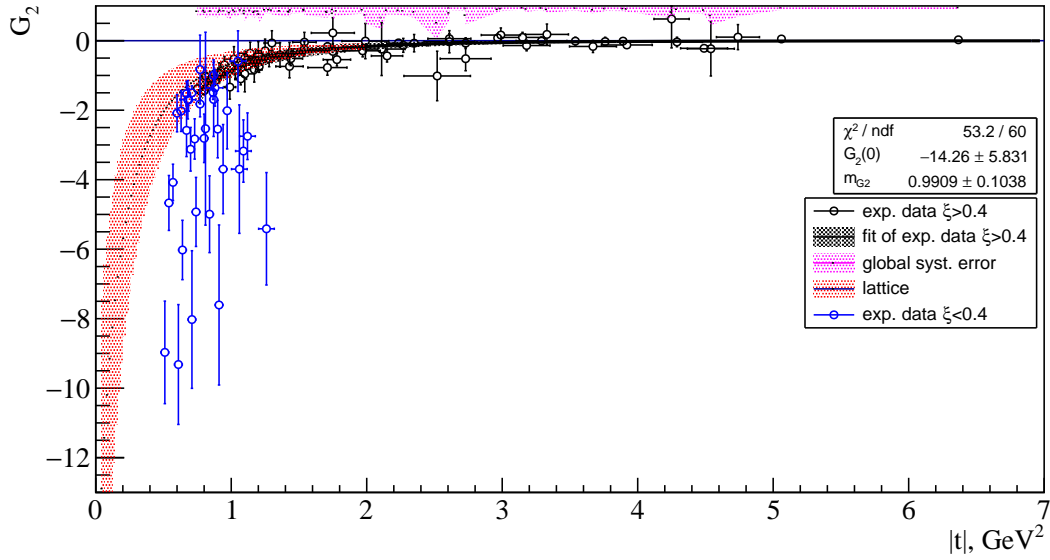
where we have defined another reduced cross section as:

$$\sigma_{R02}(E, t) = \frac{d\sigma}{dt}(E, t) \frac{\xi^4(E, t)}{F(E)(1 - \xi^2(E, t))}. \quad (19)$$

The results for the sum  $(G_0 + G_2)^{exp.}$  are shown in Fig.6, in the same way as this was done in Figs.4,5 for  $G_0^{exp.}$  and  $G_2^{exp.}$ .

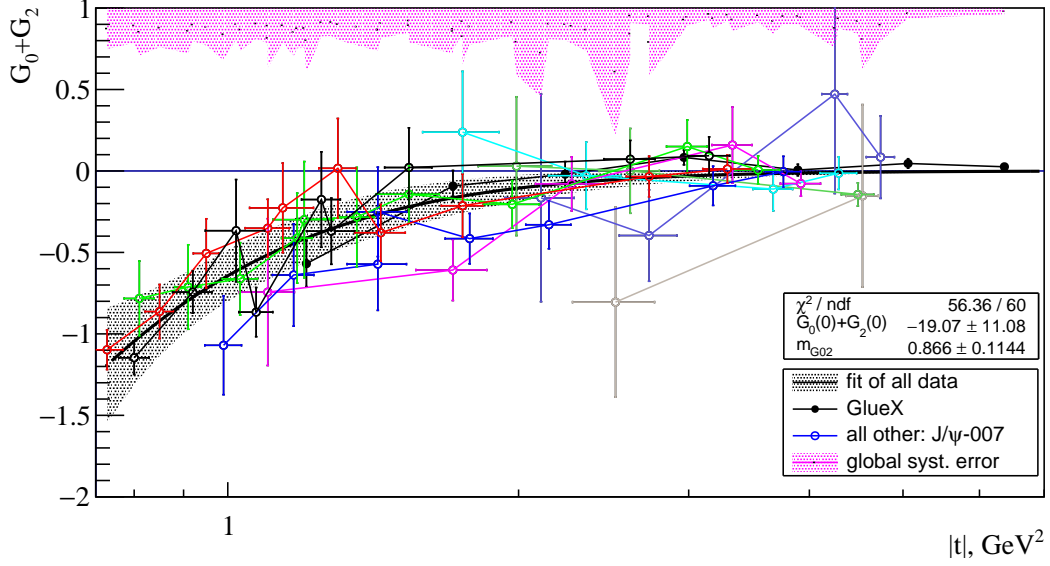


(a)

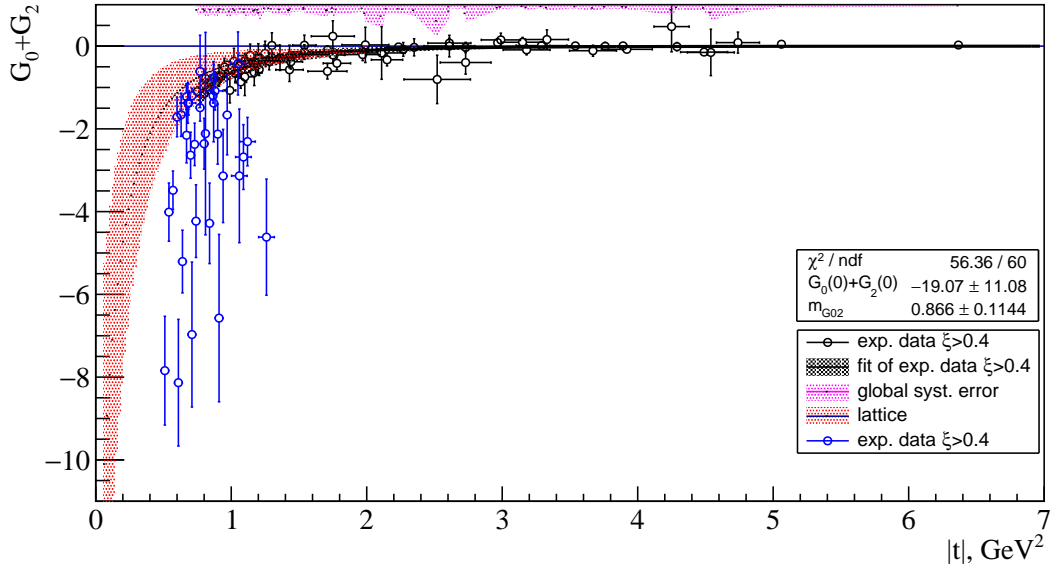


(b)

FIG. 5:  $G_0(t)$  (top) and  $G_2(t)$  (bottom) functions as extracted from the GlueX and  $J/\psi$ -007 data for  $\xi > 0.4$  and  $\xi < 0.4$  using Eqs.(9,10). The data for  $\xi > 0.4$  GeV are fitted with dipole function squared,  $G(0)/(1 - t/m_G^2)^4$ , shown with one-sigma error band. The results are compared with the calculations of  $G_0$  and  $G_2$  using the lattice results for the gGFFs in Ref. [13] in leading-moment approximation of Ref. [1].



(a)



(b)

FIG. 6: As in Figs.4,5 but for the  $G_0 + G_2$  sum, using Eq.(18). The data are fitted with a dipole function squared,  $(G_0(0) + G_2(0))/(1 - t/m_{G02}^2)^4$ .

In the leading-moment approximation, when neglecting the  $B_g$  form factor, we have:

$$G_0(t) = (2A_1^{conf})^2 A_g^2(t) \quad (20)$$

$$G_0(t) + G_2(t) = 2(2A_1^{conf} A_g(t))(8A_1^{conf} C_g(t)). \quad (21)$$

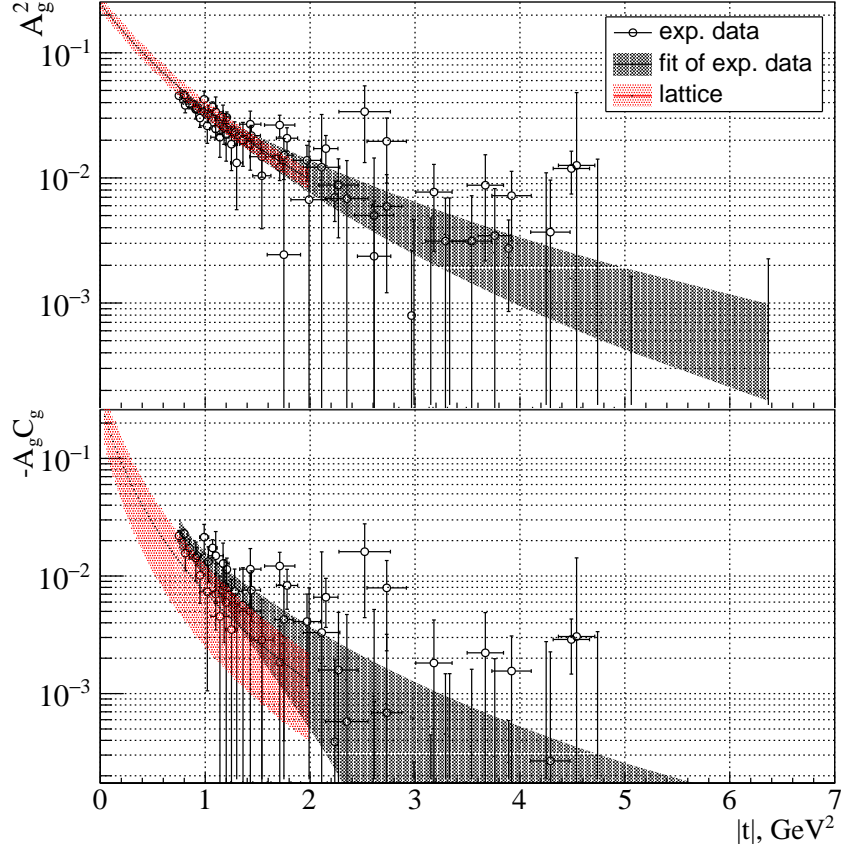


FIG. 7: The  $A_g$  form factor squared (top), and the product of the two form factors with negative sign  $-A_g C_g$  (bottom), extracted from the experimental data within the leading-moment approximation of Ref. [1], fitted with dipole functions (one-sigma error band shown) and compared to the lattice results of Ref. [13].

Thus, from the data we can extract directly  $A_g^2(t)$  and the product of the two form factors,  $A_g(t)C_g(t)$ , being proportional to  $G_0$  and  $G_0 + G_2$ , respectively. The results are shown in Fig.7.

Note that the mass scale parameter for  $G_0$  is bigger than the one for  $G_0 + G_2$ ,  $m_{G_0} > m_{G_0+G_2}$ . This means that  $C_g$  vanishes faster with  $|t|$  than  $A_g$ . Thus, in addition to the  $\xi$  suppression at low  $|t|$ , this explains qualitatively the smaller contribution of  $G_4 \sim C_g^2$  in Eq.(1) at high  $|t|$  values. Quantitatively, we have verified based on the results in this paper, that for  $|t| > 1 \text{ GeV}^2$ ,  $G_4$  is much smaller in absolute value than  $\xi^{-4}G_0$  and  $\xi^{-2}G_2$ . Thus, in the leading-moment approximation, this justifies neglecting the  $G_4$  term when extracting the form factors.

## V. ADDITIONAL REMARKS AND SUMMARY

An interesting result can be deduced from the general  $\xi$ -scaling expression, Eq.(1), though not directly related to the extraction of the form factors. First, we note that  $G_0$  must be positive as a sum of squares of gCFFs, according to Eq.(4) with  $t$  being negative. Therefore, from Eq.(9), for  $E_i > E_j$  at a fixed  $t$ , as  $\xi(E_i, t) < \xi(E_j, t)$  and therefore  $\xi^{-2}(E_i, t) - \xi^{-2}(E_j, t) > 0$ , it follows that:

$$d\sigma/dt(E_i, t) \frac{\xi^2(E_i, t)}{F(E_i)} > d\sigma/dt(E_j, t) \frac{\xi^2(E_j, t)}{F(E_j)}, \quad E_i > E_j. \quad (22)$$

In particular, as  $\xi^2(E_i, t)/F(E_i) < \xi^2(E_j, t)/F(E_j)$ , it means that:

$$d\sigma/dt(E_i, t) > d\sigma/dt(E_j, t), \quad E_i > E_j. \quad (23)$$

In other words, the differential cross section at a fixed  $t$  must increase with the energy, something that is not trivial. Based on Eq.(22) and using the same arguments in reverse we can claim from Eq.(10) that  $G_2(t) < 0$ , as  $\xi^2(E_i, t) - \xi^2(E_j, t) < 0$ . This statement however is not strict mathematically as, compared to Eq.(22), we need to take into account the additional factor of  $\xi^2$  in the reduced cross section, Eq.(11), though this effect turned out to be relatively small. In the leading-moment approximation,  $G_2(t) < 0$  would mean that  $A_g$  and  $C_g$  have opposite signs.

To summarize, our ‘‘Rosenbluth’’ procedure relies on Eq.(1) that comes in Ref. [1] from some general theoretical assumptions about the  $J/\psi$  photoproduction mechanisms, such as gluon exchange and factorization. The observation of the energy independence of the extracted  $G_0$  and  $G_2$  functions means that the experimental data, within their uncertainties, are consistent with the assumptions in Ref. [1].

We conclude, based on the analysis of the current experimental data (Fig.5), that the  $\xi$ -scaling behavior is valid for  $\xi > 0.4$ . As discussed in Ref. [1], such a low limit is not justified theoretically and may result in a significant bias. However, this value should be considered as a lower limit of the validity of the  $\xi$ -scaling, as more precise data could move this value up.

We have compared the extracted  $G_0$  and  $G_2$  functions with the calculations in the leading-moment approximation when using lattice gGFFs. Note that our procedure relies partially on the lattice constraints of the form factors when extrapolating the reference cross section to the lower  $|t|$  region. Therefore, the data points in Figs.5,7 cannot be considered independent when compared to the lattice results. In addition, the  $\xi > 0.4$  limit discussed above was also partially based on comparison with the lattice calculations. A minimization procedure was proposed that would make it possible to avoid the use of the lattice constraints, which however, requires higher statistics. More data are needed to study the region of the validity of the  $\xi$ -scaling. If with higher statistics the agreement between the data and lattice calculations in the overlapping  $t$ -region is confirmed, this could justify the extraction of the gGFFs at high  $t$  directly from the data, complementary to the lattice results available at low  $t$ .

It is critical to further investigate the near-threshold region of  $E < 9.3$  GeV. For that we would need more statistics and further theoretical and phenomenological studies to understand the possible contribution of the open charm channels. If gluon exchange still dominates at least in some kinematic region, it will be very important to have this region included in the presented analysis. It is believed that close to threshold, being close to both  $|t|_{min}$  and  $|t|_{max}$  kinematic limits, the factorization would be better justified, at the same time the higher  $\xi$  values in this region would better satisfy the requirements for the high- $\xi$  expansion in Ref.[1].

The results in this paper should not be considered as a proof of the validity of the assumptions in Ref. [1], rather just as an indication within the present data uncertainties, of the validity of the  $\xi$ -scaling as defined by Eq.(1). Nevertheless, the presented results are encouraging and should stimulate the continuation of the experimental studies and further theoretical analysis.

## VI. ACKNOWLEDGMENTS

We would like to thank Yuxun Guo for the fruitful discussions and explanations of the theory on which the results of this work are based and Simon Taylor for valuable comments.

Notice: Authored by Jefferson Science Associates, LLC under U.S. DOE Contract No. DE-AC05-06OR23177. The U.S. Government retains a non-exclusive, paid-up, irrevocable, world-wide license to publish or reproduce this manuscript for U.S. Government purposes.

---

- [1] Y. Guo, X. Ji, and F. Yuan, *Phys. Rev. D* **109**, 014014 (2024).
- [2] S. J. Brodsky and G. A. Miller, *Physics Letters B* **412**, 125 (1997).
- [3] P. Sun, X.-B. Tong, and F. Yuan, *Physics Letters B* **822**, 136655 (2021).
- [4] Y. Guo, X. Ji, and Y. Liu, *Physical Review D* **103** (2021), 10.1103/physrevd.103.096010.
- [5] Y. Guo, X. Ji, Y. Liu, and J. Yang, *Physical Review D* **108** (2023), 10.1103/physrevd.108.034003.
- [6] Y. Hatta and M. Strikman, *Phys. Lett. B* **817**, 136295 (2021).
- [7] A. Ali et al. (GlueX collaboration), *Phys. Rev. Lett.* **123**, 072001 (2019).
- [8] S. Adhikari et al. (GlueX collaboration), *Physical Review C* **108** (2023), 10.1103/physrevc.108.025201.
- [9] B. Duran et al. ( $J/\psi$ -007 collaboration), *Nature* **615**, 813 (2023).
- [10] K. A. Mamo and I. Zahed, *Phys. Rev. D* **103** (2021), 10.1103/physrevd.103.094010.
- [11] L. Frankfurt and M. Strikman, *Phys. Rev. D* **66**, 031502 (2002).
- [12] D. A. Pefkou, D. C. Hackett, and P. E. Shanahan, *Physical Review D* **105** (2022), 10.1103/physrevd.105.054509.
- [13] D. C. Hackett, D. A. Pefkou, and P. E. Shanahan, “Gravitational form factors of the proton from lattice qcd,” (2023), arXiv:2310.08484 [hep-lat].
- [14] M. N. Rosenbluth, *Phys. Rev.* **79**, 615 (1950).
- [15] M.-L. Du, V. Baru, F.-K. Guo, C. Hanhart, U.-G. Meißner, A. Nefediev, and I. Strakovsky, *Eur.Phys.J.C* **80** (2020), 10.1140/epjc/s10052-020-08620-5.
- [16] D. Winney, C. Fernández-Ramírez, A. Pilloni, A. N. Hiller Blin, M. Albaladejo, L. Bibrzycki, N. Hammoud, J. Liao, V. Mathieu, G. Montaña, R. J. Perry, V. Shastry, W. A. Smith, and A. P. Szczepaniak (Joint Physics Analysis Center), *Phys. Rev. D* **108**, 054018 (2023).
- [17] T.-J. Hou, J. Gao, T. J. Hobbs, K. Xie, S. Dulat, M. Guzzi, J. Huston, P. Nadolsky, J. Pumplin, C. Schmidt, I. Sitiwaldi, D. Stump, and C.-P. Yuan, *Phys. Rev. D* **103**, 014013 (2021).